MATERIALS SCIENCE

Grain polydispersity and coherent crystal reorientations are features to foster stress hotspots in polycrystalline alloys under load

Juan D. Ospina-Correa[1,2,3†], Daniel A. Olaya-Muñoz[2,3†‡], Juan J. Toro-Castrillón[2], Alejandro Toro[2], Abelardo Ramírez-Hernández[4], Juan P. Hernández-Ortíz[2,3]*

The mechanical properties of metallic alloys are controlled through the design of their polycrystalline structure via heat treatments. For single-phase microstructures, they aim to achieve a particular average grain diameter to leverage stress hardening or softening. The stochastic nature of the recrystallization process generates a grain size distribution, and the randomness of the crystallographic orientation determines the anisotropy of a mechanical response. We developed a multiscale computational formalism to capture the collective mechanical response of polycrystalline microstructures at unprecedented length scales. We found that for an averaged grain size, the mechanical response is highly dependent on the grain size distribution. The simulations reveal the topological conditions that promote coherent grain texturization and grain growth inhibition during stress relaxation. We identify the microstructural features that are responsible for the appearance of stress hotspots. Our results provide the elusive evidence of how stress hotspots are ideal precursors for plastic and creep failure.

INTRODUCTION

Inspired by nature, the design of next-generation advanced materials rely on the precise control of hierarchical structures composing the material. To achieve this, a fundamental understanding of the interplay between the different length scales is needed. A particularly challenging problem is to understand the complex relationship between structural evolution and topology with the material's macroscopic properties (*1*). Successful designs that adopted an ultimate control of the nano- and microstructural features, with the goal of modifying the materials crystalline structure at multiple length scales, have been reported previously (*2*–*4*).

A critical problem is to control the physical characteristics of polycrystalline aggregates during the design of microstructures toward optimized arrangements with improved mechanical properties. Concomitantly, processing conditions that allow the precise formation of microstructures are essential (*5*–*7*) to boost the development of heat treatment methodologies for high-performance applications, i.e., high-temperature, high-resistance, creep-resistant, and low-weight materials. The absence of multiscale crystallization approaches has motivated the use of single-crystal (SC) superalloys, such as those for aircraft turbine blades, where high-temperature strength and creep resistance are required (*8*). Nevertheless, manufacturing SC alloys require complex and expensive processes, thereby making this alternative unfeasible for common applications where high-resistance performance is still needed (*9*).

When a polycrystalline material is subjected to a deformation field, the stress—the load/force or strain energy—is distributed heterogeneously through the crystalline structure depending on local energy dissipation mechanisms, i.e., grain boundary (GB) migration, GB mobility, and grain rotation (*10*, *11*). In addition, zones of stress accumulation are formed around some grain neighborhoods, which are now called stress hotspots (SHSs) (*12*, *13*). After energy dissipation mechanisms are exhausted, voids are nucleated through the microstructure; they are precursors of plastic damage, crack formation and propagation, and creep. Furthermore, the crystallographic orientation of the microstructure, defined by the angle adopted by each grain during nucleation and growth, determines the anisotropic nature of the mechanical response (*14*). Creep damage is a major mechanism of failure of polycrystalline materials at high temperatures. It is a diffusion-control phenomenon that is driven by nucleation, growth, and coalescence of microscopic voids at the GBs. Typically, it is induced by the heterogeneous stress distribution in local grain neighborhoods (*15*, *16*). The prediction of creep and the engineering adaptation of the material structure for a targeted high-temperature performance require a fundamental knowledge of the microstructure, the interfaces, and the crystallographic orientations from the nanoscale (1×10^{-9} m) to the macroscale (millimeters, centimeters, or more) (*17*, *18*). Although SHSs had been proposed as the most probable locations where voids are nucleated (*13*, *19*, *20*), there is a lack of experimental and theoretical evidence that correlates them with the microstructural features of polycrystalline materials (*20*–*22*).

In this sense, experimental and theoretical setups have been proposed to characterize the main features of microstructures under load. Texture analysis through electron backscatter diffraction (EBSD) can be used to measure the evolution of the crystallographic orientation, as well as the stress and strain fields (*23*, *24*). Previous studies have shown that in situ EBSD measurements coupled to microtensile tests are a powerful tool to characterize the microstructural evolution of alloys under deformation (*25*–*27*). This methodology requires a tensile test system coupled to an EBSD detector to map the microstructural features of the sample, and it is extensible to in situ thermal exposure experiments. Although this technique captures

[1]Universidad Autónoma Latinoamericana, Facultad de Ingeniería–Grupo de Investigación INGECO, Medellín, Colombia. [2]Departamento de Materiales y Nanotecnología, Facultad de Minas, Universidad Nacional de Colombia–Medellín, Medellín, Colombia. [3]Colombia/Wisconsin One-Health Consortium, Universidad Nacional de Colombia–Medellín, Medellín, Colombia. [4]Department of Biomedical Engineering and Chemical Engineering, The University of Texas at San Antonio, San Antonio, TX 78249, USA.
†These authors contributed equally to this work.
‡Present address: Facultad de Ingeniería, Institución Universitaria Pascual Bravo, Medellín, Colombia.
*Corresponding author. Email: jphernandezo@unal.edu.co, jphernandezo@wisc.edu

the orientation evolution of loaded microstructures and provides information about the lattice strain, its use for calculation of the stress state of the entire microstructure is impractical. Experimental results are obtained in the plastic regime to facilitate the observation of textural evolution and crystal lattice rotation, although the method can be adapted for elastic conditions. Nevertheless, reproducing creep conditions, i.e., those in which an alloy is subjected to constant load at high temperature, using this experimental procedure may be unviable because of the long times required to promote appreciable topological changes and the enormous amount of electron diffraction data that the EBSD system needs to process to capture the texture evolution. These experimental constraints motivated the use of theoretical and numerical approaches not only to understand and predict the mechanical behavior of alloys under stress but also to assist and complement experimental observations under several load conditions.

Continuum mechanics and large-scale molecular dynamics (LSMD) are the preferred methods that have been selected to achieve such an elusive task. With continuum representations, the inherent inhomogeneities of the microstructure—GBs, grain topology, and orientations—cannot be taken into account explicitly, thereby limiting predictions to a macroscopic level, i.e., it is impossible to predict how the microstructure evolves as a function of the applied stress (*15*, *16*). On the other hand, atomistic descriptions, with LSMD, allow the entire reconstruction of the grain morphology, and the migration of GBs and dislocations can be measured as a function of an applied stress (*28*–*31*). Unfortunately, LSMD simulations are currently limited to systems of tens of nanometric grains that are simulated during short periods: 10^7 atoms during 10 ns (*28*, *32*).

In this work, we proposed a new multiscale—continuum/discrete—framework to simulate polycrystalline microstructures under load that allows to explicitly represent polycrystalline materials over a wide spectrum of length scales, considering thousands of micrometer-sized grains. We adopted a theoretically informed Monte Carlo (TIMC) free energy minimization formalism, where a phenomenological description of a polycrystalline structure is used, including material physical information and nonlinear elastic deformation mechanisms. During simulation, a free energy functional of a microstructure under load is minimized over the configuration space, thereby providing unique insight into the correlation between the stress field and structure topology. Our goal is to provide physical insights to understand how a microstructure evolves during the initial stages of a deformation and how the topological features determine the location of the SHSs. Our free energy functional is a modified Potts model (*33*) that considers a global dislocation density, harmonic elastic penalizations for the grain size distribution, and energy densities for two deformation mechanisms: (i) an external load applied on the entire microstructure (global strain) and (ii) local deformations given by the orientation mismatch between grains (local strain). Our polycrystalline elastic modified Potts (PEMP) free energy functional encodes elastic properties of the microstructure and takes into account long- and short-range interactions between the grain ensemble. The dislocation density is included through the energy difference between two adjacent grains given by the Read-Shockley theory, which relies on the elastic parameters of the material—elastic modulus and Poisson's ratio (*19*, *34*, *35*). Last, the elastic response of the microstructure is considered through an energy density that depends on the stiffness tensor, which is calculated with the Lamé coefficients and the crystallographic orientation of the microstructure (*10*). PEMP details and its parametrization are included in Materials and Methods and in the Supplementary Materials.

RESULTS AND DISCUSSION

In silico building up of polycrystalline aggregates

Figure 1 shows stress-free microstructures for a thermally treated American Iron and Steel Institute (AISI) 304 steel that are characterized according to the elastic energies associated with the perimeter and area of the grains (*36*). A conventional heat treatment process was used to achieve three different mean grain diameters, namely, 20, 30 and 40 μm, which were parametrized following the American Society for Testing and Materials (ASTM) E122-113 standard. The PEMP energy functional was tuned to achieve similar microstructures with the same mean grain sizes. Experimental and simulated microstructures are shown in Fig. 1 (A to C). Notice how the simulated structures are composed of equidimensional crystals that exhibit shapes of euhedral crystals with fully developed faces, i.e., a polygonal structure. We used a similarity function, through an Inverse discrete Fourier transform—the IDFT, of the optical signal generated by the GBs, and we obtained similitudes higher than 70% between simulated and experimental images. To quantify the microstructures even further, we include the grain size distributions in Fig. 1D. They are calculated by digital image analysis using plane-polarized light optical microscopy for the AISI 304 alloy. Our PEMP functional and TIMC minimization reproduces any desired mean grain size and distribution by modifying the Lagrange multipliers of the harmonic shaping functions within the functional.

The symmetry of cubic crystals determines that the relative orientations between grains can be described in 24 different forms. Conventionally, the smallest misorientation angle, θ_m, is used to describe such rotations. The maximum value of θ_m is 62.8°, while for polycrystalline structures with random orientations, θ_m has a mean value of ~45°, indicating that the structure have equant grains with polygonal shapes intersecting at triple boundaries. We measured the misorientation angle between grains in the simulated stress-free microstructures and found a consistent mean value around 45° (Fig. 1E). The probability densities of the misorientation angle, for the in silico microstructures, follow the analytical distribution for a random single-phase polycrystal, given by Mackenzie (*37*). Note that the maximum misorientation and its frequency are indicators of cubic crystal symmetries. Last, the distribution of the number of sides of the grains for all simulated structures resulted in an average of six sides in the grain local neighborhood, following Euler's theorem of polygonal aggregates (*38*). Results in Fig. 1 are strong indicators that our model reproduces polycrystalline microstructures from a local balance of the interfacial tension at the GBs. To our knowledge, our approach is the first theoretical methodology able to reproduce the size and shape of the final microstructures in good agreement with experiments (please refer to an extended discussion in the Supplementary Materials).

Texture-dependent mechanical response

The macroscopic mechanical properties of polycrystalline materials strongly depend on grain morphology, grain size distribution, and the evolution of crystallographic orientations (*14*). During an elastic response, an applied stress promotes grain growth and boosts texture evolution (large segments of grains with similar orientations),

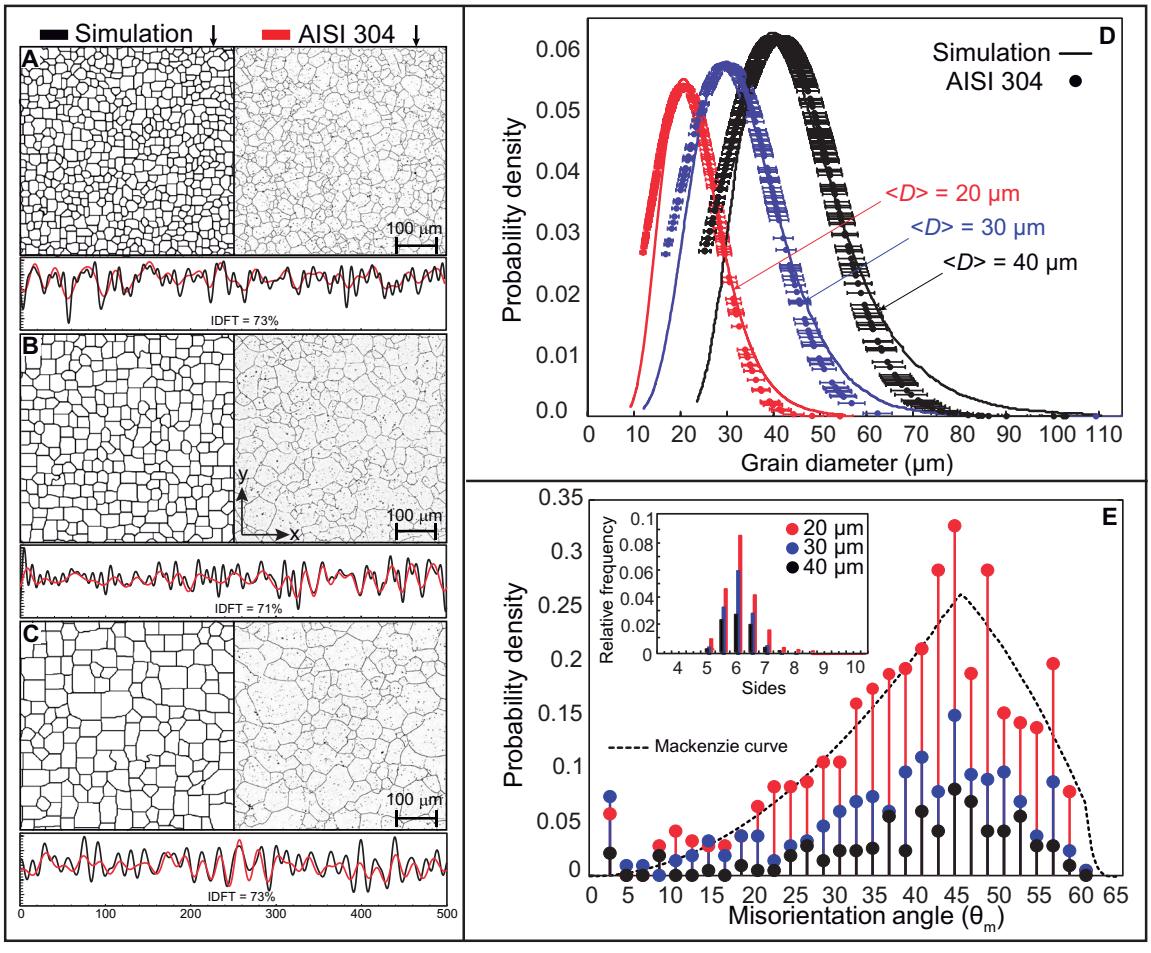

Fig. 1. Stress-free AISI 304 polygonal microstructures. Typical in silico (PEMP) and experimental digital images of microstructures with an average grain size of (**A**) $< D > =$ 20 μm (ASTM 8), (**B**) $< D > =$ 30 μm (ASTM 7), and (**C**) $< D > =$ 40 μm (ASTM 6). The inverse discrete Fourier transform (IDFT) profiles are included under the microstructures: Black lines are for the simulated structures, while the red lines are for the experimental images. Characteristics, simulated and experimental, of three different heat-treated AISI 304 steels: (**D**) grain size distributions, (**E**) misorientation angle distributions, including the theoretical predictions by Mackenzie (*37*), and an inset with the number of sides distribution.

which foster the mechanisms for the energy dissipation during the plastic response (*39*). To study how the microstructures are affected by an external load, we imposed a constant deformation along the *y* axis to all structures considering periodic boundary conditions in the *x* direction. The displacement was of 1 μm at each boundary to guarantee that the microstructure is still at the elastic regime, i.e., mean von Mises stress $<\sigma_{VM}>$ is below the yield stress $\sigma_Y = 750$ MPa (please see details behind the model parametrization in the Supplementary Materials). Although we considered a constant strain, our method can be used for constant stress. After the system is deformed, the PEMP free energy functional is minimized again using the TIMC. Figure 2 summarizes the most relevant observations after a single deformation event is applied to all the microstructures. In the figure, we include contour plots of von Mises stresses, grain orientations, and the SHS for an AISI 304 alloy with mean grain diameters of 20, 30, and 40 μm.

A notable feature to notice in Fig. 2 (A to C) is the high level of stress anisotropy driven by the orientation mismatch between each grain and the strain direction. Macroscopically, the yield stress of an alloy marks the end of the elastic regime and the beginning of the plastic deformation. Microscopically, GB migrations allow the reduction (or increase) of the yield point. In addition, for anisotropic aggregates, the elastic limit also depends on the shape of the GB, because its geometry influences stress concentrations. Therefore, a scattered elastic response in identical aggregates is expected once the orientational anisotropy of the constituent grains increases. We performed nanoindentation tests for the heat-treated AISI304 alloys (please see the details in the Supplementary Materials), and we measured a notorious change in the apparent Young's modulus for every grain in the microstructure. We included this information in our model by using a stiffness tensor that depends on the orientation of each grain.

As can be seen in Fig. 2 (A to C), our model predicts that higher stresses are located at the smaller grains, while bigger grains allow a better stress relaxation. This behavior agrees with the classical dislocation theory that states how the mobility of dislocations and GBs decreases as the grain size is reduced: strain hardening of microstructures with grain refinement (*40*). This theory had motivated the use of the mean grain size as an engineering parameter to improve the resistance of polycrystalline solids. A meaningful condition of the stress states shown in Fig. 2 (A to C, left) is the presence

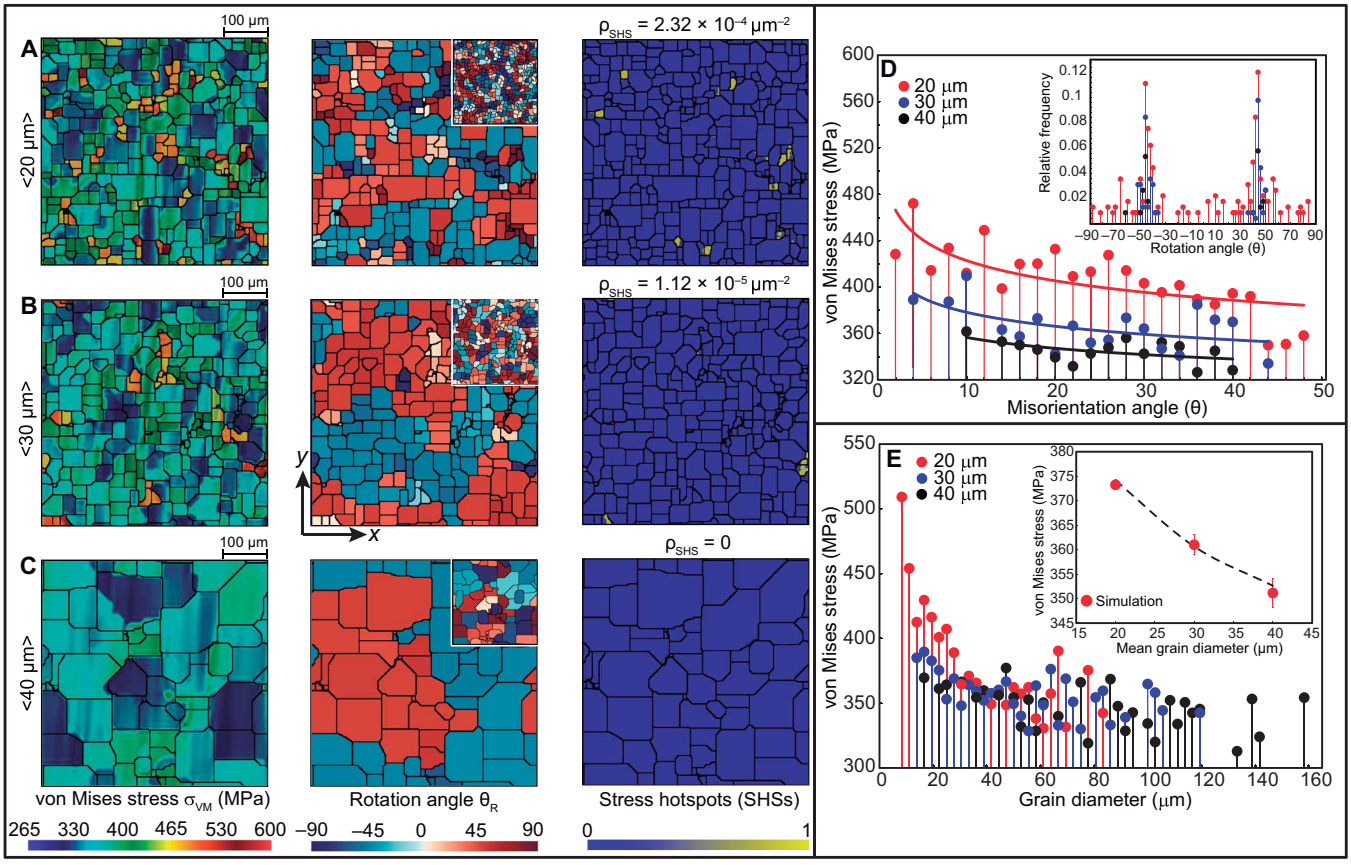

Fig. 2. Single-deformation state of the microstructures after energy minimization. The microstructure mean grain sizes are: (**A**) $< D >$ = 20 μm (ASTM 8), (**B**) $< D >$ = 30 μm (ASTM 7), and (**C**) $< D >$ = 40 μm (ASTM 6). Contours of the von Mises stresses (left), grain rotations (middle), and the isotropic threshold for SHS (yellow regions) identification (right) are shown to identify the microstructures. (**D**) Rotational coherent texture that results in polygrain zones with a similar crystallographic orientation, thereby promoting stress homogenization around ~45° relative to the load axis (inset). (**E**) von Mises stresses as a function of the grain size and the mean grain size (inset). These results reproduce the Hall-Petch softening effect.

of polygrain stress bands, as indicated by the continuity in the von Mises stresses along several grains despite the presence of GBs. Recall that the initial orientation state has no "texture," as the free energy minima for the stress-free microstructures follow the Mackenzie distribution (Fig. 1E). The differences in the crystallographic orientation between adjacent grains should result in a discontinuous stress state that follows the initial texture-free microstructure. However, during the deformed PEMP minimization, we observe that grain rotation is the most active energy dissipation mechanism, driving a notorious change in the crystallographic orientation, as shown in Fig. 2 (A to C, middle). Once the deformed state reaches the energy minimum, the microstructures present a coherent preferred orientation that spans multiple grains. These textured structures promote stress homogenization. To our knowledge, this is the first direct simulation that enables the direct correlation between the stress state and the coherent texturizing process of a microstructure. In Fig. 2D, we show the stress as a function of the grain misorientation angle; featuring (i) a monotonic increase of the mean stress (fitted curve) as the mean grain size is decreased and (ii) monotonic decrease of the mean stress (fitted curve) as the misorientation angle is increased. We also found that the prevalent rotation angle is ~45° with respect to the load axis [see Fig. 2 (D, inset)]. We believe that the activation of the grain rotation mechanism emulates the sliding-planes process that promotes plastic flow. Let us expand around these observations and hypothesis. As the misorientation angle decreases, the GB mobility is also reduced, thereby inhibiting the grain growth as a mechanism for stress relaxation. The stagnation of grain growth notably increases the stress state for smaller grains, while for microstructures with larger grains, the stress dependence on the misorientation angle is virtually inexistent. This is consistent with the misorientation-dependent Read-Shockley theory of recrystallization during deformation (*41*, *42*).

Our results show that regardless of the macroscopic stress relaxation, some grains are unable to reduce their stress state. We use an ideal threshold based on the mechanical response of an isotropic alloy with the same mechanical properties, i.e., every point on the microstructure that exceeds the von Mises stress of the isotropic structure is identified as an SHS. Figure 2 (A to C, right) shows the threshold contours for the three AISI 304 alloys. The yellow marks determine the presence of the SHS: stress accumulation zones. Notice that there is a monotonic reduction of the SHS as the mean grain size increases. We quantify this in Fig. 2E, where the von Mises stress is plotted as a function of the grain size and as a function of the mean grain size (inset). Our predictions agree with experimental

evidence based on the softening of alloys with bigger grain sizes: the Hall-Petch effect (*43*–*45*). The length scales—10^2 to 10^4 grains—considered in our model allow the direct identification of the SHSs and their correlation with grain topology.

Engineering control of SHSs

The versatility and simplicity of our model allow a straightforward control of the grain size distribution. For instance, we evaluate the effect of a nonlinear elastic deformation on microstructures with a mean grain diameter of 20 μm but with different grain size distributions (SD). The idea is to use the microstructure with the smallest grain size, the candidate for a high-performance application, and to study how the grain size distribution affects the density of SHS and the mechanical response. Figure 3A shows predesigned grain size distributions defined with SDs of σ_{M1} = 4.291 μm (black color), σ_{M2} = 8.089 μm (red color) (original distribution in Fig. 2), and σ_{M3} = 14.31 μm (blue color). Simulated microstructures, including the stress and SHS densities, for a single deformation event of 1 μm are shown in Fig. 3 (B to D). The values of the density of SHS, defined as the number of SHSs per unit area, are included for completeness. The number of SHSs decreases as the grain size distribution includes the presence of "bigger" grains. In other words, there is an active strain-hardening mechanism for microstructures with monodispersed distributions while softening in microstructures with wider distributions. An interesting feature to discuss is how the distribution affects the evolution of the microstructure under stress. In the inset in Fig. 3A, we show that the grain growth of the microstructures after the stress was imposed. In addition, in Fig. 3E, we plot the von Mises stress as the function of the deformed grain microstructure.

The lower stress state is observed for the wider distributed microstructure, i.e., σ_{M3} = 14.31 μm, which also exhibits the larger grain growth after deformation. Consequently, the average von Mises stress decreases as the SD of the original microstructure increases (see inset in Fig. 3E). There is a direct correlation between the number of SHSs, the hardening/softening, and the initial distribution of the microstructure. This is quantified by the ~150-MPa difference in the von Mises stress between structures with σ_{M1} = 4.291 μm and σ_{M3} = 14.31 μm. Consequently, according to our simulations, to control the mean grain size is not sufficient for the design of high-performance alloys. The homogeneity in grain size ensures the strain hardening of the structure, while a heterogeneous structure promotes stress relaxation through grain growth and a softer response, which are useful for high-toughness and high-ductility applications.

We found that SHSs are formed in small grains with low misorientations, which agrees with previous observations (*13*, *26*, *46*). The

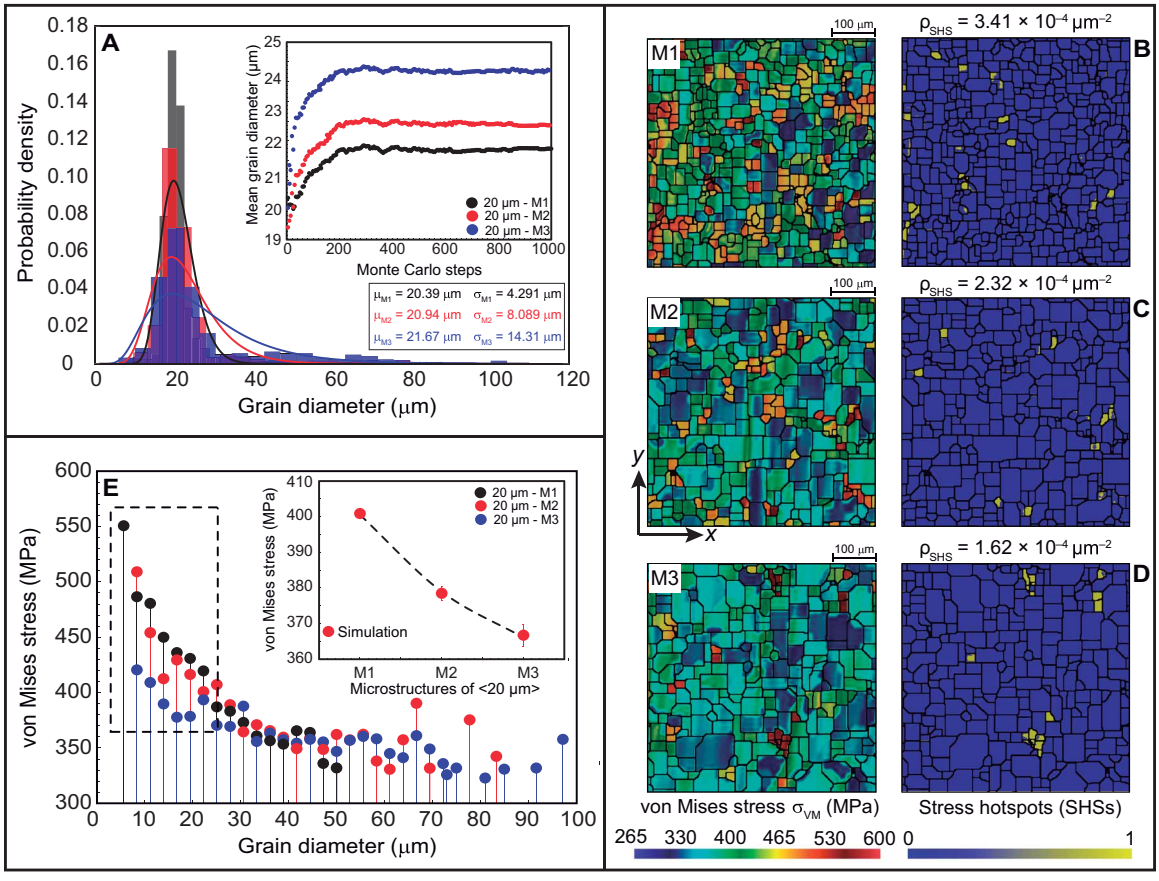

Fig. 3. Mechanical response and SHSs for microstructures with different grain size distributions. (**A**) Generated grain size distributions, where the red line is the original distribution presented previously. The black line corresponds to the M1 microstructure, where the grain diameter is more homogeneous than the M2 microstructure, and the blue line represents the size distribution of the M3 microstructure, where the variance in grain size is higher than in the M1 and M2 microstructures. (**B** to **D**) Right: Stress profile for the three different microstructures. (**E**) Reduction in the presence of the von Mises as the function of the microstructure and inset in (E) representing the growth of the different microstructures under the stress conditions.

presence of smaller grains not only influences the microstructural evolution around their neighborhood but also promotes a long-range mechanical response because their GB mobility is restricted. Nevertheless, our model reveals that size is not enough to produce SHSs. We found that the misorientation angle controls the level of interaction between the smaller grains and their neighborhood. A small misorientation angle inhibits GB migration and grain growth. The stagnation of the grain growth also deactivates the crystal rotation mechanism, thereby delaying the coherent texturization process. It is the interplay between misorientations, GB migration, and the coherent texturization that direct the emergence of SHSs: (i) Small grains with an effective texturization are able to reduce their stress state, while (ii) small grains with restrained rotation accumulate stress. For instance, in the case of microstructures with some degree of crystalline anisotropy, such as the ones typically found in engineering alloys, where a combination of cubic, tetragonal, and hexagonal crystal structures is present, we would expect a variation in the GB mobility due to a change in the misorientation distribution function. This modification may alter the grain diffusive behavior under stress by increasing the emergence of SHSs, for a decreased GB mobility, or, conversely, by reducing the SHS concentration once the GB mobility increases. We summarize these conclusions in Fig. 4. In the figure, we include a deformed microstructure with a mean grain size of 20 μm and σ_{M1} = 4.291 μm. Three zones with small grains are highlighted, and the required conditions to relieve an accumulated stress are described during a free energy relaxation. We observe how grain growth facilitates the relaxation of the stress state. Nevertheless, coherent texturization favors stress reduction in a local neighborhood where the GB mobility is restrained. Once the final rotation angle, within a grain, diverges from the maximum shear stress direction [~45° (*47*)], the SHS is promoted. These local regions lead up to nucleation and coalescence of voids. It is straightforward to conclude that a higher density of SHS will accelerate the damage rate, thereby placing them as candidates for plastic failure and creep precursors.

Microstructural characterization of polycrystalline solids under deformation has been limited because of a lack of experimental methods able to capture this multiscale phenomenon. Through a novel theoretical platform, we control the morphology and size of polycrystalline aggregates, not only to reproduce the microstructural features of austenitic metallic alloys but also to replicate any polygonal structure. By simulating a large number of grains, we can correlate stress relaxation to coherent textural formation, grain topology, and distribution. We determine the conditions for SHSs to appear in the deformed microstructure. In particular, our results show how the macroscopic stress response depends on the interplay between the crystallographic orientations and the local grain size topology. We found that small grains with restrained rotations—low misorientation angles—accumulate stress, thereby promoting zones for stress accumulation (SHS). Concomitantly, the modification of the initial grain size distribution function of a microstructure, while preserving its mean diameter, provides a route for engineering control over the emergence of SHSs. The grain size distribution can be used to predesign and adjust the hardening/softening ratio of the mechanical response of polycrystalline alloys for high-performance applications. The model and results presented in this research offer an unprecedented mesoscopic view of polycrystalline aggregates under stress conditions and foster a theoretically aided design platform for the new generation of metallic alloys.

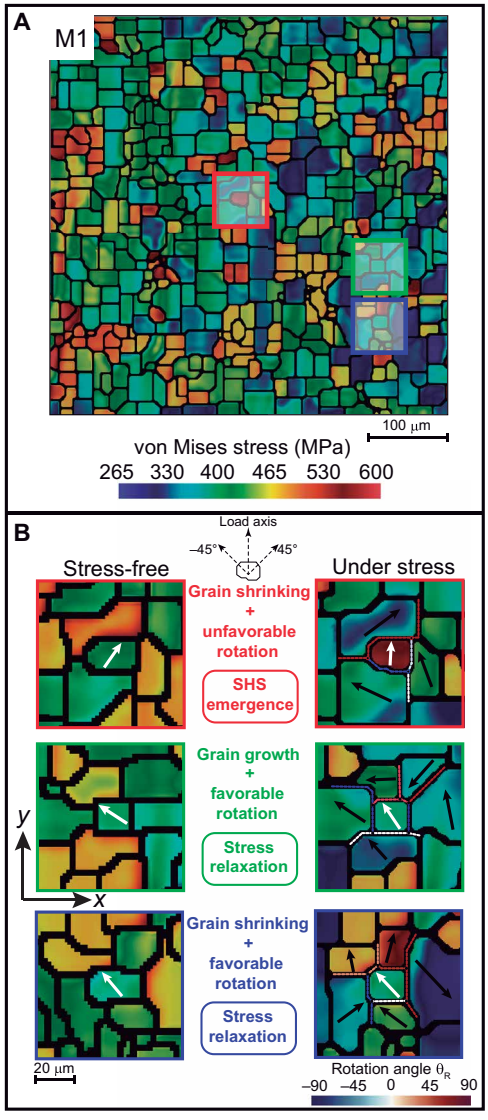

Fig. 4. Mechanisms for SHSs: Misorientations, GB migration, and coherent texturizations. (**A**) Contour of the von Mises stress σ_{VM} for a microstructure with an initial mean grain size of 20 μm and σ_{M1} = 4.291 μm. Three zones with small grains are highlighted: (red) with an SHS after deformation and (green and blue) with stress relaxation after deformation. (**B**) Relaxation mechanisms to induce (or not) an SHS. Smaller grains can shrink (red and blue), favoring the growth of neighboring grains, or they can grow in a preferred direction (green) directed by GB mobility. However, it is the activation of the rotation mechanism toward the maximum shear stress direction (±45°), which allows the stress relief. White arrows illustrate the rotation angle θ_R of the central grain, while the black arrows represent the orientation of its neighbors. We color the GB of the neighborhood to show the misorientation angle between grains.

MATERIALS AND METHODS

Free energy functional and TIMC

Our free energy functional is composed of two fundamental contributions: (i) a polycrystalline modified Potts model, $\mathcal{H}_{PM}$, and (ii) an elastic density that considers the external deformation field and the presence of the grain boundaries, $\mathcal{H}_E$. We call this free energy functional a PEMP model, and it is written as follows

$$\mathcal{H} = \Big[\sum_{i=1}^{N}\sum_{j=1}^{\Gamma_i}\gamma_{ij}(1-\delta_{ij}) + \sum_{k=1}^{N_g}\lambda(s_k)(s_k - S_T)^2 + \sum_{k=1}^{N_g}\sigma(v_k)(v_k - V_T)^2\Big] + \frac{1}{2}\Big[\sum_{i=1}^{N}\left(\boldsymbol{\varepsilon}_i^T:\mathbf{C}_i:\boldsymbol{\varepsilon}_i\right) + \delta_{GB}\left(\nabla\theta_i^T:\mathbf{C}_i:\nabla\theta_i\right)\Big] \quad (1)$$

where N is the number of lattice points of the system, Γ_i are the neighbors of each lattice, and N_g is the number of grains of the microstructure. The $\mathcal{H}_{PM}$, first bracket, is composed of three energy densities, namely, for the crystallographic orientations, the perimeter, and the area of the grains. The free energy penalization over the grain orientation is done through the γ_{ij} parameter and the Kronecker-like delta function δ_{ij}, which is one of two neighboring lattices that have the same crystallographic orientation and zero otherwise. Harmonic energy densities are used to set the area and perimeter of the grains, where the Lagrange multipliers, $\lambda(s_k)$ and $\sigma(v_k)$, are not constants in our model and S_T and V_T are the targeted grain perimeter and area, respectively. The H_E, second bracket, depends on the local stiffness tensor $\mathbf{C}$, which is a function of the Lamé parameters of the material and the crystallographic orientation of the grains. The external deformation field determines the global strain field, $\boldsymbol{\varepsilon}$, while the local strain field $\nabla\theta$ includes the deformation of the crystalline lattices due to the presence of a grain boundary with thickness δ_{GB} (please refer to fig. S3 for a detailed graphical representation of our free energy functional).

Our simulations are performed in two-dimensional crystalline structures of 500 μm by 500 μm. We use a coarse grain description of the crystalline system, where the microstructure is discretized using a squared lattice. The resolution of the "mesh" is determined according to the ratio between the minimum and maximum length scale of the desired microstructure. In this work, we selected cubic crystalline structures for an AISI 304 steel with grains between 5 and 100 μm that covered near 1-mm length scales. We performed consistency and stability analyses and found that around 160,000 lattice points were sufficient to resolve the system. For this particular case, each lattice point represents 10^8 atoms. The TIMC free energy minimizations were carried out in 5 to 10 independent simulations. Every simulation started from a randomly generated crystalline structure with more than 40,000 grains. The grain size was defined according to (i) a circle of equivalent radius, $r = (A_{grain}/\pi)^{1/2}$, (ii) using the ASTM E112-113, and (iii) an averaged grain diameter ($< D >$) through the arithmetic mean value of Feret axis in the grain. We evaluated and compared the statistical reliability of the grain size distribution with the results of the distributions obtained from experimental results for an austenitic stainless steel AISI 304 that was heat-treated to achieve grain size distributions with three different mean diameters—20, 30, and 40 μm. Using the software ImageJ v.1.50b, it was possible to get two-dimensional graphs of the intensities of pixels along a line within each microstructure. The inverse Fourier transform was implemented and correlated with the signal between AISI 304 and the theoretical results.

The TIMC starts with a Metropolis scheme to generate a Markov chain. In particular, random trial updates of the local crystal orientation (CO) and rotations are proposed and accepted according to the Metropolis criteria. We established the grain rotation (with a maximum value of 2° per trial) and the probability of reorientation of a selected lattice following a uniform probability distribution to guarantee detailed balance. For deformation conditions, the change in CO is driven by hydrostatic stress, increasing the probability of reorientation in tensile zones while allowing stagnation in compressive zones, following the mechanisms established by Stress-assisted diffusion. We constructed a Markov chain of these configurations by proposing transitions between an old configuration and a new one with probability $P(\text{old} \rightarrow \text{new}) = \min[1, \exp(-\beta\Delta\mathcal{H})]$ (where $\beta^{-1} = k_B T$, $\Delta\mathcal{H} = \mathcal{H}_{new} - \mathcal{H}_{old}$, T is the temperature, and k_B is Boltzmann constant). To guarantee the energy minimization without local entrapment, we included rotation-coalescence mechanisms into the Markov chain: (i) a grain k is selected randomly and a small rotation in every Euler's angle is proposed; if the CO of the kth grain matches with some neighboring grain, then the probability of coalescence increases, (ii) grain k and grain l are selected randomly and a small rotation is performed for every CO, and the neighborhood of each grain will be checked to verify the coalescence between adjacent grains (two or more). Stress-free minimizations required more than 10^3 Monte Carlo (MC) steps, where each step is defined as N-lattice random trials. Deformed structures were minimized an additional 600 MC steps (for a more detailed representation of our deformation scheme, we refer the reader to fig. S7).

Materials and characterization

We used an AISI 304 austenitic stainless steel (19.2 mm round bar; hardness, 270 HV) with polycrystalline structure. The steel was heat-treated in an electric furnace in air at temperatures of 1000°, 1050°, and 1100°C for 10 min and rapidly quenched in water to achieve three different microstructures. Every specimen was prepared following a standard procedure that includes grinding with emery papers and polishing in napped microfiber cloths using 1-μm diamond suspension and 0.03-μm alumina suspension. The microstructure was revealed using electrochemical etching using a solution of 65% HNO_3 in ethanol, with current density between 0.04 and 0.06 A/cm^2, voltage between 1.5- and 2.0-V DC, and pure titanium as the cathode. The etching time varied between 180 and 300 s depending on the mean size of the grain. Micrographs were obtained using a Nikon Eclipse LV100 optical microscope; an automated digital imaging system was implemented to measure the grain size distribution of each sample using the software ImageJ v.1.50b, through plane-polarized light optical microscopy reflected-light mode. The photographs were analyzed with a plane-polarized light optical microscopy reflected light (Carl Zeiss AXIO SCOPE-A1-POL, high-resolution, chromatic correction with objectives of 5, 10, 20, 50, and 100× in air) following the method described in ASTM D2799 standard adapted for inorganic materials. The recognition of the polycrystalline structures in the polished sections allowed the identification of ~2500 grains per section with a confidence interval of 95%, ensuring the reliability of the results with an excellent statistical approach. Last, variables such as area, perimeter, Feret diameter, shape, and circularity were used to evaluate the grain size distribution.

Nanoindentation

The AISI 304 stainless steel specimens were heat-treated in an electric furnace at 1100°C for 15 min and quenched in water to achieve a mean grain diameter of 50 μm. Then, a stress-relieving treatment was carried out at 700°C. We selected nine different zones of 180 μm by 180 μm to carry out nanoindentation tests to measure the mechanical response of the alloy. We used an Ibis Authority nanoindenter, by Fischer-Cripps Laboratories, with a modified-Berkovich diamond tip. We conducted the load cycle using a closed-loop control up to a maximum load of 20 mN for 5 s. The load was then reduced

to 2% of the maximum load for an additional 5 s. The separation between adjacent indentations was ~15 μm to avoid distortions in the measure caused by plastic deformation. The indentation depth was around 400 nm to inhibit the bulk effect produced by grains beneath the surface. Last, we obtained the apparent elastic modulus $\widetilde{E}$ from the load-unload curve using the Hertzian theory of contact mechanics. We averaged the measured values in the zones to obtain a distribution function of $\widetilde{E}$ to include the mean value as an input in the deformation simulation.

SUPPLEMENTARY MATERIALS

Supplementary material for this article is available at http://advances.sciencemag.org/cgi/content/full/7/15/eabe3890/DC1

REFERENCES AND NOTES

1. V. R. Vedula, S. J. Glass, D. M. Saylor, G. S. Rohrer, W. C. Carter, S. A. Langer, E. R. Fuller Jr., Residual-stress predictions in polycrystalline alumina. *J. Am. Ceram. Soc.* **84**, 2947–2954 (2001).
2. S. Yip, M. P. Short, Multiscale materials modelling at the mesoscale. *Nat. Mater.* **12**, 774–777 (2013).
3. M. Stoykovich, M. Muller, S. Kim, H. Solak, E. Edwards, J. De Pablo, P. Nealey, Directed assembly of block copolymer blends into nonregular device-oriented structures. *Science* **308**, 1442–1446 (2005).
4. X. Li, J. A. Martínez-González, J. P. Hernández-Ortiz, A. Ramírez-Hernández, Y. Zhou, M. Sadati, R. Zhang, P. F. Nealey, J. J. de Pablo, Mesoscale martensitic transformation in single crystals of topological defects. *Proc. Natl. Acad. Sci. U.S.A.* **114**, 10011–10016 (2017).
5. S. E. Offerman, N. H. van Dijk, J. Sietsma, S. Grigull, E. M. Lauridsen, L. Margulies, H. F. Poulsen, M. T. Rekveldt, S. van der Zwaag, Grain nucleation and growth during phase transformations. *Science* **298**, 1003–1005 (2002).
6. L. Margulies, G. Winther, H. Poulsen, In situ measurement of grain rotation during deformation of polycrystals. *Science* **291**, 2392–2394 (2001).
7. M. Tonks, P. Millett, Phase field simulations of elastic deformation-driven grain growth in 2D copper polycrystals. *Mater. Sci. Eng. A* **528**, 4086–4091 (2011).
8. T.-K. Tsao, A.-C. Yeh, C.-M. Kuo, K. Kakehi, H. Murakami, J.-W. Yeh, S.-R. Jian, The high temperature tensile and creep behaviors of high entropy superalloy. *Sci. Rep.* **7**, 12658 (2017).
9. T. M. Pollock, Alloy design for aircraft engines. *Nat. Mater.* **15**, 809–815 (2016).
10. J. M. Dake, J. Oddershede, H. O. Sørensen, T. Werz, J. C. Shatto, K. Uesugi, S. Schmidt, C. E. Krill III, Direct observation of grain rotations during coarsening of a semisolid Al-Cu alloy. *Proc. Natl. Acad. Sci. U.S.A.* **113**, E5998–E6006 (2016).
11. Q. P. Kong, Q. F. Fang, Progress in the investigations of grain boundary relaxation. *Crit. Rev. Solid State* **41**, 192–216 (2016).
12. M. A. S. Qidwai, A. C. Lewis, A. B. Geltmacher, Using image-based computational modeling to study microstructure–yield correlations in metals. *Acta Mater.* **57**, 4233–4247 (2009).
13. A. Mangal, E. A. Holm, Applied machine learning to predict stress hotspots II: Hexagonal close packed materials. *Int. J. Plast.* **114**, 1–14 (2019).
14. R. Ahluwalia, T. Lookman, A. Saxena, Elastic deformation of polycrystals. *Phys. Rev. Lett.* **91**, 055501 (2003).
15. R. Brenner, R. A. Lebensohn, O. Castelnau, Elastic anisotropy and yield surface estimates of polycrystals. *Int. J. Solids Struct.* **46**, 3018–3026 (2009).
16. C. J. Hamelin, B. J. Diak, A. K. Pilkey, Multiscale modelling of the induced plastic anisotropy in bcc metals. *Int. J. Plast.* **27**, 1185–1202 (2011).
17. A. D. Orme, I. Chelladurai, T. M. Rampton, D. T. Fullwood, A. Khosravani, M. P. Miles, R. K. Mishra, Insights into twinning in Mg AZ31: A combined EBSD and machine learning study. *Comput. Mater. Sci.* **124**, 353–363 (2016).
18. K. Rajan, Materials informatics: The materials gene and big data. *Annu. Rev. Mat. Res.* **45**, 153–169 (2015).
19. D. L. Olmsted, S. M. Foiles, E. A. Holm, Survey of computed grain boundary properties in face-centered cubic metals: I. Grain boundary energy. *Acta Mater.* **57**, 3694–3703 (2009).
20. A. D. Rollett, R. A. Lebensohn, M. Groeber, Y. Choi, J. Li, G. S. Rohrer, Stress hot spots in viscoplastic deformation of polycrystals. *Model. Simul. Mat. Sci. Eng.* **18**, 074005 (2010).
21. M. Ardeljan, M. Knezevic, T. Nizolek, I. J. Beyerlein, N. A. Mara, T. M. Pollock, A study of microstructure-driven strain localizations in two-phase polycrystalline HCP/BCC composites using a multi-scale model. *Int. J. Plast.* **74**, 35–57 (2015).
22. F. Willot, L. Gillibert, D. Jeulin, Microstructure-induced hotspots in the thermal and elastic responses of granular media. *Int. J. Solids Struct.* **50**, 1699–1709 (2013).
23. T. Zhang, D. M. Collins, F. P. E. Dunne, B. A. Shollock, Crystal plasticity and high-resolution electron backscatter diffraction analysis of full-field polycrystal Ni superalloy strains and rotations under thermal loading. *Acta Mater.* **80**, 25–38 (2014).
24. V. V. C. Wan, M. A. Cuddihy, J. Jiang, D. W. MacLachlan, F. P. E. Dunne, An HR-EBSD and computational crystal plasticity investigation of microstructural stress distributions and fatigue hotspots in polycrystalline copper. *Acta Mater.* **115**, 45–57 (2016).
25. S. Li, C. Guo, L. Hao, Y. Kang, Y. An, In-situ EBSD study of deformation behaviour of 600 mpa grade dual phase steel during uniaxial tensile tests. *Mater. Sci. Eng. A* **759**, 624–632 (2019).
26. W. Zhang, J. Lu, J. Wang, L. Sang, J. Ma, Y. Zhang, Z. Zhang, In-situ EBSD study of deformation behavior of inconel 740h alloy at high-temperature tensile loading. *J. Alloys Compd.* **820**, 153424 (2020).
27. T. E. Buchheit, J. D. Carroll, B. G. Clark, B. L. Boyce, Evaluating deformation-induced grain orientation change in a polycrystal during in situ tensile deformation using EBSD. *Microsc. Microanal.* **21**, 969–984 (2015).
28. E. A. Holm, S. M. Foiles, How grain growth stops: A mechanism for grain-growth stagnation in pure materials. *Science* **328**, 1138–1141 (2010).
29. G. Agarwal, A. M. Dongare, Deformation twinning in polycrystalline Mg microstructures at high strain rates at the atomic scales. *Sci. Rep.* **9**, 3350 (2019).
30. L. A. Zepeda-Ruiz, A. Stukowski, T. Oppelstrup, V. V. Bulatov, Probing the limits of metal plasticity with molecular dynamics simulations. *Nature* **550**, 492–495 (2017).
31. Y. Shibuta, S. Sakane, E. Miyoshi, S. Okita, T. Takaki, M. Ohno, Heterogeneity in homogeneous nucleation from billion-atom molecular dynamics simulation of solidification of pure metal. *Nat. Commun.* **8**, 10 (2017).
32. X. Ke, J. Ye, Z. Pan, J. Geng, M. F. Besser, D. Qu, A. Caro, J. Marian, R. T. Ott, Y. M. Wang, F. Sansoz, Ideal maximum strengths and defect-induced softening in nanocrystalline-nanotwinned metals. *Nat. Mater.* **18**, 1207–1214 (2019).
33. F. Graner, J. A. Glazier, Simulation of biological cell sorting using a two-dimensional extended potts model. *Phys. Rev. Lett.* **69**, 2013–2016 (1992).
34. A. J. Haslam, D. Moldovan, V. Yamakov, D. Wolf, S. R. Phillpot, H. Gleiter, Stress-enhanced grain growth in a nanocrystalline material by molecular-dynamics simulation. *Acta Mater.* **51**, 2097–2112 (2003).
35. D. Moldovan, V. Yamakov, D. Wolf, S. R. Phillpot, Scaling behavior of grain-rotation-induced grain growth. *Phys. Rev. Lett.* **89**, 206101 (2002).
36. J. Wejchert, D. Weaire, J. P. Kermode, Monte Carlo simulation of the evolution of a two-dimensional soap froth. *Philos. Mag. B* **53**, 15–24 (2006).
37. J. K. Mackenzie, Second paper on statistics associated with the random disorientation of cubes. *Biometrika* **45**, 229–240 (1958).
38. C. V. Thompson, Grain growth and evolution of other cellular structures. *Solid State Phys.* **55**, 269–314 (2001).
39. R. Goswami, C. R. Feng, S. B. Qadri, C. S. Pande, Fatigue-assisted grain growth in Al alloys. *Sci. Rep.* **7**, 10179 (2017).
40. Z. C. Cordero, B. E. Knight, C. A. Schuh, Six decades of the hall-petch effect – A survey of grain-size strengthening studies on pure metals. *Int. Mater. Rev.* **61**, 495–512 (2016).
41. M. C. Theyssier, J. H. Driver, Recrystallization nucleation mechanism along boundaries in hot deformed Al bicrystals. *Mater. Sci. Eng. A* **272**, 73–82 (1999).
42. S. Biswas, I. Samajdar, A. Haldar, A. Sain, Coarsening in polycrystalline material using quaternions. *J. Phys. Condens. Matter* **23**, 072202 (2011).
43. J. Schiøtz, F. D. Di Tolla, K. W. Jacobsen, Softening of nanocrystalline metals at very small grain sizes. *Nature* **391**, 561–563 (1998).
44. J. Schiøtz, T. Vegge, F. D. Di Tolla, K. W. Jacobsen, Atomic-scale simulations of the mechanical deformation of nanocrystalline metals. *Phys. Rev. B* **60**, 11971–11983 (1999).
45. C. S. Pande, K. P. Cooper, Nanomechanics of hall-petch relationship in nanocrystalline materials. *Prog. Mater. Sci.* **54**, 689–706 (2009).
46. A. Mangal, E. A. Holm, Applied machine learning to predict stress hotspots I: Face centered cubic materials. *Int. J. Plast.* **111**, 122–134 (2018).
47. R. A. Lebensohn, A. K. Kanjarla, P. Eisenlohr, An elasto-viscoplastic formulation based on fast Fourier transforms for the prediction of micromechanical fields in polycrystalline materials. *Int. J. Plast.* **32-33**, 59–69 (2012).
48. A. C. Oates, N. Gorfinkiel, M. González-Gaitán, C.-P. Heisenberg, Quantitative approaches in developmental biology. *Nat. Rev. Genet.* **10**, 517–530 (2009).
49. L. Wang, J. Teng, P. Liu, A. Hirata, E. Ma, Z. Zhang, M. Chen, X. Han, Grain rotation mediated by grain boundary dislocations in nanocrystalline platinum. *Nat. Commun.* **5**, 4402 (2014).
50. J. Luo, V. K. Gupta, D. H. Yoon, Segregation-induced grain boundary premelting in nickel-doped tungsten. *Appl. Phys. Lett.* **87**, 231902 (2005).
51. M. Nygards, Number of grains necessary to homogenize elastic materials with cubic symmetry. *Mech. Mater.* **35**, 1049–1057 (2003).
52. B. M. Schroeter, D. L. McDowell, Measurement of deformation fields in polycrystalline OFHC copper. *Int. J. Plast.* **19**, 1355–1376 (2003).

53. M. Kamaya, Y. Kawamura, T. Kitamura, Three-dimensional local stress analysis on grain boundaries in polycrystalline material. *Int. J. Solids Struct.* **44**, 3267–3277 (2007).
54. M. Kamaya, Measurement of local plastic strain distribution of stainless steel by electron backscatter diffraction. *Mater Charact* **60**, 125–132 (2009).
55. D. A. Olaya-Muñoz, P. F. Nealey, J. P. Hernández-Ortiz, Leveling of polymer grating structures upon heating: Dimension dependence on the nanoscale and the effect of antiplasticizers. *ACS Appl. Mater. Interfaces* **10**, 27432–27443 (2018).

Acknowledgments
Funding: This study was funded by the Universidad Nacional de Colombia–Medellín, Empresas Públicas de Medellín (Central La Sierra), and COLCIENCIAS through its National Doctoral Program Scholarship. In addition, we thank the Graduate Student Scholarship and Technology and Materials Design Laboratory at Universidad Nacional de Colombia for the financial and logistical support. J.D.O.-C. is grateful to the Universidad Autónoma Latinoamericana (Facultad de Ingenierías) for the financial support. D.A.O.-M. and J.D.O.-C. are thankful to the Pritzker School of Molecular Engineering, at the University of Chicago, and the Department of Materials Science and Engineering, at Northwestern University, for scholarship program that allowed them to spend two semesters in Chicago. **Author contributions:** J.D.O.-C. and D.A.O.-M. performed the simulations and calculations included in this report. J.J.T.-C. and A.T. designed and performed the heat treatment and electrochemical etching and performed the image reconstruction and analysis of the micrographs and the nanoindentation test for the metallic alloy. A.R.-H., A.T., and J.P.H.-O. directed the discussions required to derive the model and the required experimental setups. J.P.H.-O. conceived and guided the research. All authors contributed to the data analysis and manuscript preparation. **Competing interests:** The authors declare that they have no competing interests. **Data and materials availability:** All data needed to evaluate the conclusions in the paper are present in the paper and/or the Supplementary Materials. Additional data related to this paper may be requested from the authors.

Submitted 18 August 2020
Accepted 22 February 2021
Published 9 April 2021
10.1126/sciadv.abe3890

Citation: J. D. Ospina-Correa, D. A. Olaya-Muñoz, J. J. Toro-Castrillón, A. Toro, A. Ramírez-Hernández, J. P. Hernández-Ortíz, Grain polydispersity and coherent crystal reorientations are features to foster stress hotspots in polycrystalline alloys under load. *Sci. Adv.* **7**, eabe3890 (2021).